JACS
JOURNAL OF THE AMERICAN CHEMICAL SOCIETY

Article

pubs.acs.org/JACS

Systematic Tuning and Multifunctionalization of Covalent Organic Polymers for Enhanced Carbon Capture

Zhonghua Xiang,[†] Rocio Mercado,[‡] Johanna M. Huck,[#] Hui Wang,[†] Zhanhu Guo,[§] Wenchuan Wang,[†,∥] Dapeng Cao,[*,†] Maciej Haranczyk,[⊥] and Berend Smit[*,‡,#,⊗]

[†]State Key Lab of Organic−Inorganic Composites, Beijing University of Chemical Technology, Beijing 100029, P.R. China

[‡]Department of Chemistry, University of California, Berkeley, Berkeley, California 94720-1462, United States

[§]Department of Chemical and Biomolecular Engineering, University of Tennessee, Knoxville, Tennessee 37996, United States

[∥]International Research Center for Soft Matter, Beijing University of Chemical Technology, Beijing 100029, P.R. China

[⊥]Computational Research Division, Lawrence Berkeley National Laboratory, Berkeley, California 94720-8139, United States

[#]Department of Chemical and Biomolecular Engineering, University of California, Berkeley, Berkeley, California 94720-1462, United States

[⊗]Institut des Sciences et Ingénierie Chimiques, Valais, Ecole Polytechnique Fédérale de Lausanne (EPFL), Rue de l'Industrie 17, CH-1951 Sion, Switzerland

Supporting Information

ABSTRACT: Porous covalent polymers are attracting increasing interest in the fields of gas adsorption, gas separation, and catalysis due to their fertile synthetic polymer chemistry, large internal surface areas, and ultrahigh hydrothermal stabilities. While precisely manipulating the porosities of porous organic materials for targeted applications remains challenging, we show how a large degree of diversity can be achieved in covalent organic polymers by incorporating multiple functionalities into a single framework, as is done for crystalline porous materials. Here, we synthesized 17 novel porous covalent organic polymers (COPs) with finely tuned porosities, a wide range of Brunauer−Emmett−Teller (BET) specific surface areas of 430−3624 m^2 g^{-1}, and a broad range of pore volumes of 0.24−3.50 cm^3 g^{-1}, all achieved by tailoring the length and geometry of building blocks. Furthermore, we are the first to successfully incorporate more than three distinct functional groups into one phase for porous organic materials, which has been previously demonstrated in crystalline metal−organic frameworks (MOFs). COPs decorated with multiple functional groups in one phase can lead to enhanced properties that are not simply linear combinations of the pure component properties. For instance, in the dibromobenzene-lined frameworks, the bi- and multifunctionalized COPs exhibit selectivities for carbon dioxide over nitrogen twice as large as any of the singly functionalized COPs. These multifunctionalized frameworks also exhibit a lower parasitic energy cost for carbon capture at typical flue gas conditions than any of the singly functionalized frameworks. Despite the significant improvement, these frameworks do not yet outperform the current state-of-art technology for carbon capture. Nonetheless, the tuning strategy presented here opens up avenues for the design of novel catalysts, the synthesis of functional sensors from these materials, and the improvement in the performance of existing covalent organic polymers by multifunctionalization.

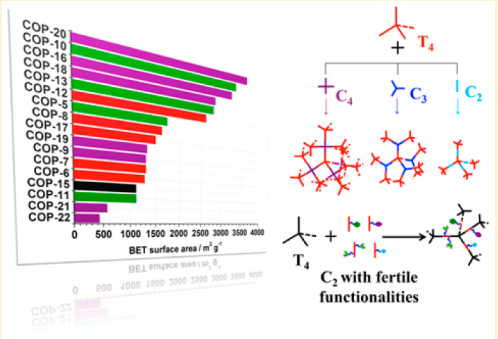

INTRODUCTION

Reducing anthropogenic carbon dioxide emission has become one of the most important social and environmental challenges facing our planet today. Due to a continued increase in the total use of fossil fuels in the foreseeable future, an essential contribution to the reduction of carbon dioxide in the atmosphere is the development of efficient carbon-capture technologies.[1] CO_2 adsorptive capture by nanoporous materials is attracting attention due to its potential to significantly reduce the energy requirements for this process.[2] Among these materials, porous covalent polymers[3] are a promising class because of their ultrahigh hydrothermal stabilities and high-yielding synthetic polymer chemistry. Unlike metal organic frameworks (MOFs), these materials only contain light elements (C, N, O, H, etc.). Although much progress has been made in manipulating the sequential arrangement of monomer units in a polymer chain, conventional polymer synthetic approaches tend to produce materials with an unsatisfying porous nature (e.g., low specific surface area (SSA) and small pore volume).[4] Determining how to best control the porous properties of these statistically polymerized

Received: June 23, 2015
Published: September 27, 2015

DOI: 10.1021/jacs.5b06266
J. Am. Chem. Soc. 2015, 137, 13301−13307

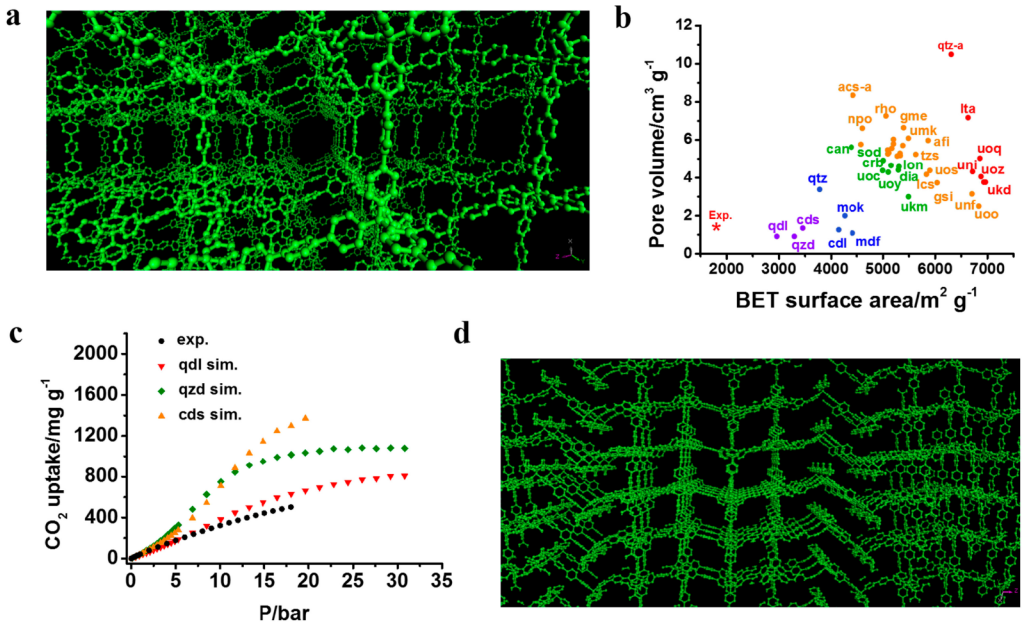

Figure 1. Screening hypothetical COP-5 structures using atomistic simulations. (a) Structure of COP-5 with diamond topology generated *in silico*. (b) Scatterplot illustrating BET surface area versus pore volume for the COP-5 structures with different topologies generated *in silico*, along with the experimental result. (c) Comparison of computed CO_2 isotherms in COP-5 with the **qdl**, **qzd**, and **cds** topologies, with the experimental results at 298 K. (d) Structure of COP-5 with **qdl** topology generated *in silico*.

materials in a similar fashion to crystalline MOFs[5] and covalent organic frameworks (COFs)[6] remains a great challenge.

Recently, Cooper and co-workers employed Sonogashira–Hagihara coupling chemistry to prepare a series of conjugated microporous polymers (CMPs) with controllable surface areas and pore dimensions by varying the monomer length.[7] Nonetheless, the BET SSAs of these CMPs are still relatively low (512–1018 m^2 g^{-1}). Although it has been shown that having alkynyl functional groups in covalent polymer networks can lead to cross-linked structures, it has also been shown that three-dimensional alkynyl polymers generally have higher surface areas than two-dimensional polymers.[8] In this work, we show how using the efficient Ullmann cross-coupling reaction with a combination of three-dimensional and two-dimensional linkers can lead to polymers with increased surface areas. Using the novel tuning strategy presented here, we synthesized 17 novel multiblock covalent organic polymers (COPs) with finely tuned porosities by tailoring the length and geometry of the building blocks. These synthesized multiblock COPs exhibit a wide BET SSA range of 430–3624 m^2 g^{-1} and a large pore volume range of 0.24–3.50 cm^3 g^{-1}.

As the number of different materials that can be synthesized and fully tested is small compared to the total number of materials, in the spirit of the Material Genomic Initiative (MGI),[9] we used a computational approach to enumerate a large number of possible materials and predict their performance using molecular simulations. We use this approach to elucidate a relationship between the various linkers, the attainable topologies, and a material's capacity for carbon dioxide.

RESULTS

The nickel(0)-catalyzed Yamamoto-type Ullmann cross-coupling reaction is an efficient method for obtaining highly condensed networks of quasi-ordered porous organic polymers.[10] Recently, both Ben et al.[3e,11] and Yuan et al.[3f] used a tetrahedral monomer, tetrakis(4-bromophenyl) methane (TBM), to synthesize two similar quasi-ordered porous covalent polymers: a porous aromatic framework, PAF-1, with a high surface area of 5640 m^2 g^{-1}, and a porous polymer network, PPN-4, with an even higher surface area of 6461 m^2 g^{-1}. These findings motivated us to employ TBM as a core monomer, which can be connected with other rigid monomers to form tunable covalent polymers. Unfortunately, the synthesized COP-5 (see vide infra for the related characterization of as-synthesized COP-5) prepared with TBM and 1,4-dibromobenzene (DB) exhibits a much lower surface area, 1744 m^2 g^{-1}, than the theoretically predicted value, 5302 m^2 g^{-1}, for COP-5 with the diamond topology (Figure 1a). However, the long linkers between two neighboring core monomers allow other topologies to form. To investigate how to avoid the formation of these competing structures, we screened the porosities of COP-5 with more than 46 different crystalline topologies (Figure 1b and Table S2) and verified the predicted CO_2 adsorption isotherms with experimental results (Figure 1c). Although the synthesized materials are not necessarily crystalline, from a computational point of view, crystalline models are more easily constructed than amorphous models and thus we used such models to allow for a quicker, simpler screening of the materials. Furthermore, previous work on polymer porous networks[12] has shown how experimental measurements of gas adsorption in these and similar classes of materials can be reproduced in simulations using crystalline models, e.g., N_2 adsorption isotherms for PAF-1[3e] and CH_4 adsorption for PPN-4.[12a] These examples illustrate that these models give a sensible representation of these materials, and for these reasons, we assume a crystalline order in our model structures. Our initial models suggested that this was only a viable assumption for COP-5, as simple (i.e., noninterpenetrated, crystalline) models for other COPs we looked at (COP-10, -11, -12, -13, -14) possessed significantly larger surface areas and pore volumes compared to the synthesized materials

DOI: 10.1021/jacs.5b06266
J. Am. Chem. Soc. 2015, 137, 13301–13307

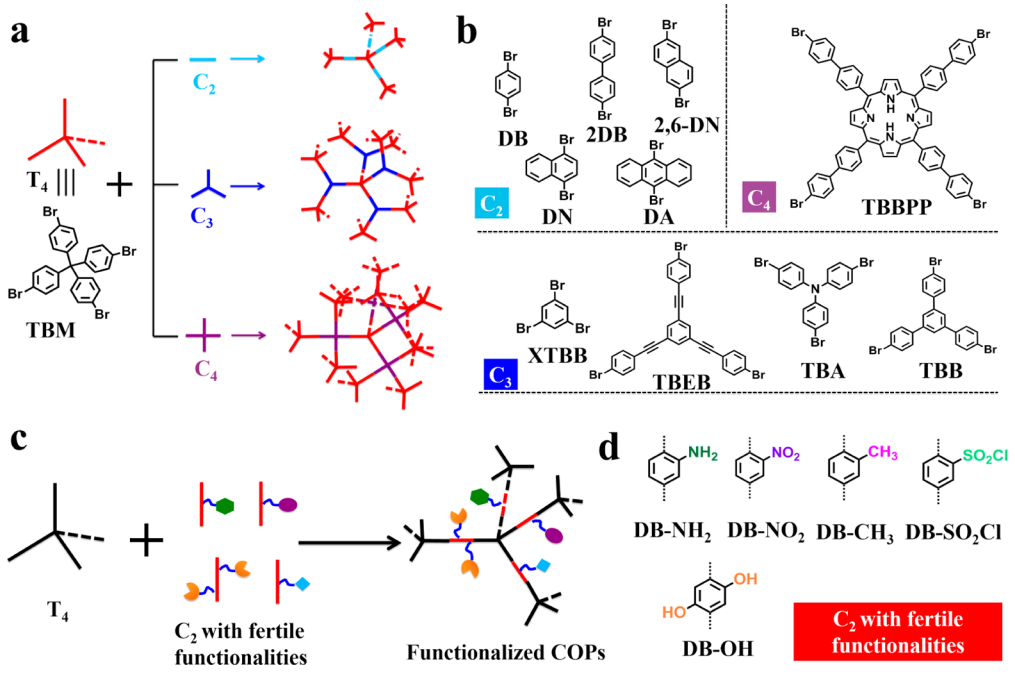

Figure 2. The scheme for porosity manipulation and functionalization in multiblock COPs. (a) The porosity of the polymers was tuned by connecting TBM with linkers of three distinct geometries. (b) The C_2, C_3, and C_4 comonomers. (c) Strategy for functionalization of the COPs. (d) The C_2 comonomers with multiple functionalities used in this work.

Table 1. Summary of the Porosities and CO_2 Capture Performance of COPs in This Work

materials	monomer 1	monomer 2	monomer 3	monomer 4	BET SSA[a] (m^2/g)	Langmuir SSA (m^2/g)	pore volume[b] (cm^{32}/g)	micropore volume[c] (cm^{32}/g)	CO_2 capacity[d] (mg g^{-1})	N_2 capacity[e] (mg g^{-1})	parasitic energy[f] (kJ/kg)	selectivity[g]
COP-5		DB			1744	2569	1.40	0.70	503	41		
COP-6		2DB			1279	1882	1.09	0.51	453	37		
COP-7		DA			1305	1916	1.18	0.41	345	31		
COP-8		2,6-DN			1634	2396	1.33	0.55	525	52		
COP-9		DN			1305	1907	0.92	0.56	352	35		
COP-10		XTBB			3337	4984	2.25	1.32	896	79		
COP-11		TBEB			1112	1654	1.09	0.33	332	34		
COP-12		TBA			2609	3852	1.86	0.98	770	66		
COP-13	TBM	TBB			2787	4123	1.91	1.11	680	57		
COP-15		TBBPP			1112	1638	0.93	0.44	421	40		
COP-16		DB−NO_2			3233	4794	2.34	1.38	797	66		
COP-17		DB−NH_2			1505	2193	1.02	0.66	446	42	1831	8.4
COP-18		DB−CH_3			2828	4157	1.83	0.58	694	56	2766	4.8
COP-19		DB−SO_2Cl			1330	1943	0.95	0.58	445	37	2009	7.8
COP-20		DB−OH			3624	5431	3.50	1.24	767	66	2615	4.5
COP-21		DB−OH	DB-NH_2		568	844	0.47	0.26	219	24	1608	13.7
COP-22		DB−OH	DB-NH_2	DB-SO_2Cl	430	617	0.21	0.21	203	20	1632	13.3

[a]The BET SSAs were calculated in the region of P/P_0 = 0.05−0.3. SSAs = specific surface areas. [b]Determined at P/P_0 = 0.9997. The pore volume in this work refers to the total pore volume including the surface condensation. [c]The micropore volume derived using the t-plot method based on the Halsey thickness equation. [d]The CO_2 uptake at 298 K and 18 bar. [e]The N_2 uptake at 298 K and 18 bar. [f]Parasitic energy for the cost of carbon capture from a 14:86 CO_2:N_2 gas mixture at 40 °C and 1 atm. [g]The IAST-predicted adsorption selectivity at 313 K and 1 atm. TBM = Tetrakis(4-bromophenyl)methane; DB = 1,4-dibromobenzene; 2DB = 4,4′-dibromobiphenyl; DA = 9,10-dibromoanthracene; 2,6-DN = 2,6-dibromonaphthalene; DN = 1,4-dibromonaphthalene; XTBB = 1,3,5-tribromobenzene; TBEB = 1,3,5-tris((4-bromophenyl)-ethynyl)benzene; TBA = tris(4-bromophenyl)amine; TBB = 1,3,5- tris(4-bromophenyl)benzene; TBBPP = 5,10,15,20-terakis-(4′-bromo-biphenyl-4-yl)−porphyrin; DB-NO_2 = 1,4-dibromo-2-nitrobenzene; DB-NH_2 = 2,5-dibromoaniline; DB-CH_3 = 2,5-dibromotoluene; DB-SO_2Cl = 2,5-dibromobenzenesulfonyl chloride; DB−OH = 2,5-dibromohydroquinone.

regardless of the topologies we considered. It is possible that due to their length and flexibility, the longer linkers lead to other properties which we did not consider in our models. Nonetheless, in agreement with previous results, we found that the shorter linkers in COP-5 led to more favorable properties for CO_2 capture and separation, as they avoid the creation of too much "empty space" in the structures. For COP-5 our molecular simulation results indicate a comparable agreement with the experimental data. For example, the CO_2 isotherms in COP-5 with **qdl** topology (RCSR[13] symbol **qdl**; Figure 1d) could well reproduce the experimental results, confirming the

DOI: 10.1021/jacs.5b06266
J. Am. Chem. Soc. 2015, 137, 13301−13307

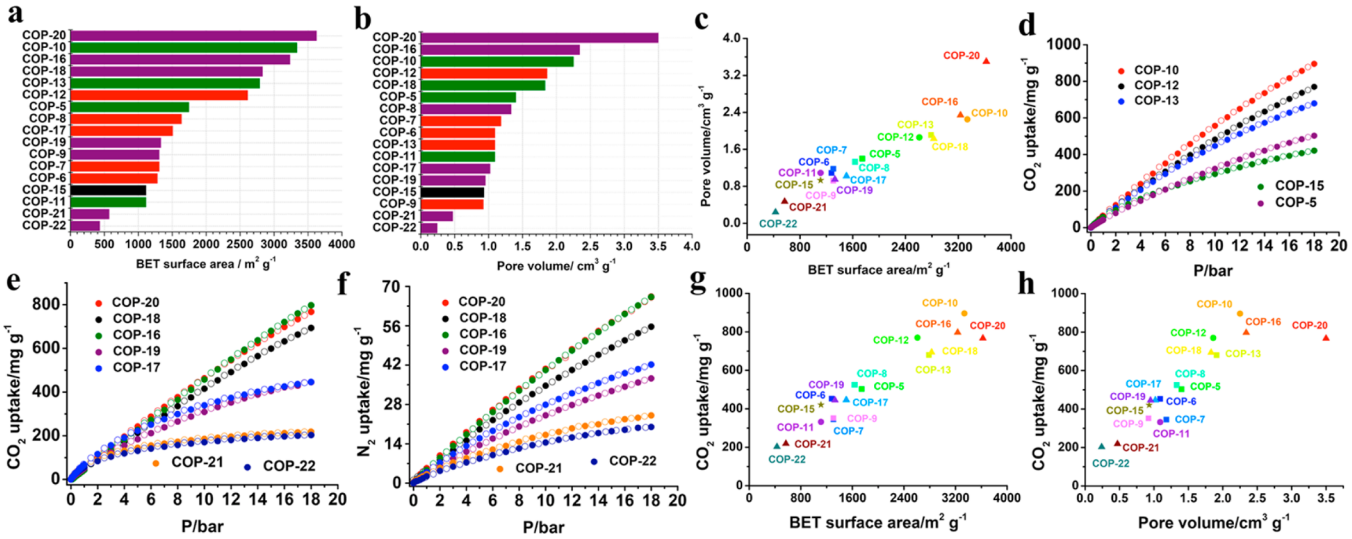

Figure 3. The porosities of the as-synthesized multiblock COPs in this study and their gas adsorption performance at 298 K. (a) BET surface area results for a series of COPs. (b) Pore volume results for a series of COPs. (c) BET specific surface area versus pore volume in a series of COPs. (d) CO_2 adsorption in nonfunctionalized COPs. (e) CO_2 adsorption in functionalized COPs. (f) N_2 adsorption in functionalized COPs. Solid and open symbols represent adsorption and desorption amounts, respectively. (g) BET specific surface area versus CO_2 storage capacity at 18 bar. (h) Pore volume versus CO_2 storage capacity at 18 bar.

success of copolymerization in the multiblock COPs using Yamamoto-type Ullmann cross-coupling.

Encouraged by these results, we further used TBM as a core monomer to copolymerize with other extended building blocks of different lengths and geometries (C_2, C_3, and C_4) to synthesize a series of multiblock COPs (Figure 2a). The geometries and lengths of the comonomers (Figure 2b) enabled us to tailor the porosities of these as-synthesized multiblock COPs, similar to the way that the porosity is tuned in crystalline MOFs.[14]

Fourier transform infrared (FT-IR) spectroscopy and solid state ^{13}C CP/MAS NMR measurements confirm the successful phenyl−phenyl coupling in this series of multiblock COPs, and the preservation of the comonomer backbones in each multiblock COP (Figures S1−S14). The powder X-ray diffraction spectra (PXRD; Figures S15 and S16) and transmission electron microscopy (TEM) images (Figures S17 and S18) suggest these multiblock COPs exhibit long-range amorphous features and tend to form spherical morphologies (Figures S19 and S20). Our synthesized multiblock COPs exhibit high thermal stability and show negligible deterioration at up to 500 °C (Figures S21 and S22). In particular, only 20% weigh loss occurs at up to 800 °C for all of the as-synthesized multiblock COPs.

We further measured the N_2 adsorption isotherms at 77 K to evaluate the porosities of these multiblock COPs (Figure S23). The results are summarized in Table 1. These results show that the porosities can be systematically tuned by tailoring the geometry and length of the comonomers. For example, the pore-size distributions of the as-synthesized multiblock COPs constructed with T_4 and C_2 monomers show a well-defined dependence on the length and geometry of the C_2 monomers (Figures S23). It is worth mentioning that the multiblock COPs constructed with the T_4 and C_3 building blocks exhibit a highly porous nature, except in the case of 1,3,5-tris((4-bromophenyl)-ethynyl)benzene (TBEB) since the alkynyl functional group tends to form cross-linked structures which reduce its porous capacity.[8] Most notably, COP-10, which is copolymerized from TBM and 1,3,5-tribromobenzene (TBB), possesses an extremely high BET SSA of 3337 $m^2\ g^{-1}$ and a pore volume of 2.25 $cm^3\ g^{-1}$, which are among the largest in the field of covalent organic materials,[3a] and even larger than those of similar analogues, such as multiblock polymers of intrinsic microporosity (PIMs)[15] and CMPs.[16]

To introduce functional groups into COPs, we functionalized C_2 monomers with various functional groups, including −OH, $-NH_2$, $-NO_2$, $-CH_3$, $-SO_2Cl$, and copolymerized these monomers with TBM (Figure 2c,d). The backbones of these functionalized COPs are characterized using similar techniques (Figures S24−S38). Whereas most reported synthetic techniques focus on a single functional group, the methodology introduced in this work allows us to incorporate more than two different functional groups.[17] We simultaneously incorporated two and three comonomers, 2,5-dibromoaniline (DB-NH_2), 2,5-dibromohydroquinone (DB−OH), and 2,5-dibromobenzenesulfonyl chloride (DB-SO_2Cl), along with TBM into one phase using a one-pot method to prepare a bifunctionalized COP-21 (−OH + $-NH_2$) and multifunctionalized COP-22 (−OH + $-NH_2$ + $-SO_2Cl$). These functionalized COPs also exhibit high porosities. In particular, COP-20 possesses an extremely high BET SSA of 3624 $m^2\ g^{-1}$ and a pronounced pore volume of 3.50 $cm^3\ g^{-1}$. The pore volume of 3.5 $cm^3\ g^{-1}$ is the largest ever reported in the field of covalent organic materials to our best of knowledge,[3a] close to the benchmark of 4.4 $cm^3\ g^{-1}$ for MOF NU-100E to date.[5b]

Generally, a high SSA and a large pore volume in a porous material often correlate with a high gas uptake.[18] By tailoring both the lengths and geometries of the building blocks, we can synthesize COPs with wide range of BET SSAs (from 430 to 3624 $m^2\ g^{-1}$, Figure 3a) and a large range of pore volumes (from 0.24 to 3.50 $cm^3\ g^{-1}$, Figure 3b). Interestingly, the BET SSAs of these COPs depend linearly on the pore volumes (Figure 3c).

The CO_2 and N_2 adsorption isotherms in these multiblock COPs are presented in Figure 3d,f. Of these COPs, COP-10 exhibits the highest CO_2 uptake of 896 mg g^{-1} at 298 K and 18

DOI: 10.1021/jacs.5b06266
J. Am. Chem. Soc. 2015, 137, 13301−13307

bar, which places it among the top ten materials with the highest CO_2 storage capacity in the field of MOFs and COFs under similar conditions to date.[19] This uptake is much larger than in its analogues under similar conditions [COF-8 (502 mg g^{-1}), COF-5 (441 mg g^{-1}), and COF-10 (412 mg g^{-1}) reported by Furukawa et al.;[20] PPN-2 (486 mg g^{-1}) and PPN-1 (393 mg g^{-1}) reported by Lu et al.;[8b] BCMBP (100) (585 mg g^{-1}) reported by Dawson et al.;[21] and PAF-1 (876 mg g^{-1}) reported by Ben et al.[3e]] and very close to the threshold of COF-103 (1038 mg g^{-1}) under similar conditions.[20]

An instructive first check to gain insights on the suitability of these functionalized multiblock COPs for their application in carbon capture is to estimate their CO_2/N_2 selectivities. For this reason, we also measured the N_2 adsorption isotherms at 298 K (Figure 3f). Likewise, N_2 adsorption capacity largely correlates with surface area and pore volume. COP-20 possesses the largest surface area and pore volume among the functionalized multiblock COPs, and it shows the highest N_2 uptake of 66 mg g^{-1} at 18 bar and 298 K.

We used Ideal Adsorbed Solution Theory (IAST) developed by Myers and Prausnitz[22] to predict the CO_2:N_2 gas mixture adsorption in each COP at a gas composition of 14:86, 40 °C and 1 atm, which corresponds to typical flue gas from a coal fired power plant at adsorption conditions relevant for a postcombustion process. Adsorption isotherms of the pure components were fit by single- and dual-site Langmuir equations with satisfactory agreement (see Figure S39). The final floating parameters are given in the Supporting Information (Table S5). The resulting selectivities of the six COPs under investigation are listed in Table 1. At first glance, none of the analyzed structures stand out in their calculated selectivities, which range from 4.5 to 13.7. However, both materials tethered with multiple functional groups perform better than the singly functionalized polymers. With decreasing selectivities follow the $-NH_2$ and $-SO_2Cl$ functionalized materials, with polymers functionalized with $-CH_3$ and $-OH$ groups performing the worst.

Evaluating materials for their application in carbon capture solely on the basis of their selectivity results does not provide a true picture of the materials' performance. As shown in previous work[2b] and other literature,[23] individual material properties, such as uptake, selectivity, and working capacity are not sufficient in the ranking procedure for a postcombustion process. Instead, a combination of these criteria is more appropriate. A potential means to evaluate materials for carbon capture is using the parasitic energy (PE). This model, based on the minimization of the energy penalty additionally imposed on a power plant by applying carbon capture and sequestration, was first introduced by Rochelle et al.[24] The advantages of this metric, compared to the previously mentioned criteria, are that it is not only the combination of several thermodynamic properties, but also that the optimization of the process conditions depend on a material-by-material basis. Figure 4 shows the rankings of the six analyzed COPs in comparison to other known materials. COPs 17−22 are illustrated as orange circles and are among the average performers. Similar to the selectivity results, COP-18 and COP-20 ($-CH_3$ and $-OH$ functionalized) performed the worst, exhibiting the largest parasitic energies of 2766 and 2615 kJ/kg_{CO2}. The $-SO_2Cl$ and $-NH_2$ functionalized materials, COP-19 and COP-17, perform 24−34% better than COP-18. A further improvement in performance is observed in the multifunctionalized COP-22 and COP-21 (PEs: 1631 and 1608 kJ/kg_{CO2}). Interestingly,

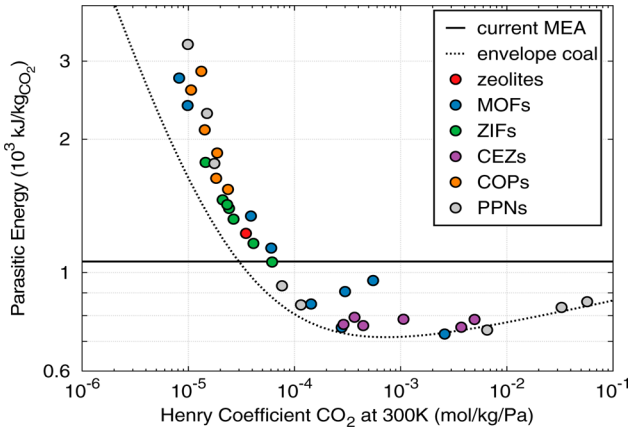

Figure 4. Parasitic energy as a function of the Henry coefficient at 300 K. The black solid line illustrates the performance of the current state-of-art technology, amine-scrubbing (1060 kJ/kg CO_2). The black dashed line depicts the performance envelope line for coal flue gas of the all-silica zeolites investigated by Lin et al.[25] The COPs under investigation in this work are marked as orange circles. The other materials are based on the results of Huck et al.[2b]

these multifunctionalized covalent organic polymers containing functional groups ($-SO_2Cl$ and $-NH_2$) demonstrated better parasitic energies than the singly functionalized COPs. It must be pointed out, however, that the most promising material analyzed in this work exhibits a parasitic energy twice as high as the best performing material discovered thus far. Thus, despite improvements upon singly functionalized COPs, COP-21 displays a greater parasitic energy cost than the current state-of-art technology, amine-scrubbing (solid line in Figure 4). The numerical values of the parasitic energies for the COPs can be found in Table 1.

An important observation can be made by examining the PPN-6 series in Figure 4. PPNs possess very similar framework structures to COPs. Thus, studying the improvements in performance within this series achieved by gradually functionalizing the framework can provide interesting insights for the related class of COPs. The performance of PPN-6 can be improved significantly from bare PPN-6 (~2290 kJ/kg_{CO2}) by converting it into either the lithium salt analogue (~934 kJ/kg_{CO2}) or the sulfonic acid grafted one (~846 kJ/kg_{CO2}), as well as by functionalizing it with various different amine groups, i.e., PPN-6-CH_2DETA, PPN-6-CH_2TAEA, and PPN-6-CH_2TETA (860, 835, and 742 kJ/kg_{CO2}).[2b] Similar parasitic energy improvements may also be expected by integrating elongated amine chains into the various COP frameworks. Therefore, these results illustrate how incorporating multiple functional groups within a single COP can lead to a significant improvement in the carbon capture properties of nanoporous materials.

CONCLUSION

We have proposed a systematic strategy for preparing multifunctionalized covalent organic polymers (COPs). Using this strategy, we have synthesized 17 novel multiblock COPs with finely tuned porosities. The COPs synthesized in this work have remarkably high porosities and hydrothermal stabilities, which are critical for the adoption of these materials for industrial applications. By tailoring the length and geometry of building blocks, we can tune the BET SSAs and pore volumes of these COPs. As a result, we have synthesized a material,

DOI: 10.1021/jacs.5b06266
J. Am. Chem. Soc. 2015, 137, 13301−13307

COP-20, with the largest measured pore volume in the field of porous organic materials, 3.5 $cm^3\ g^{-1}$. Our synthetic approach also allows us to incorporate different functional groups into COPs; we have successfully incorporated 5 distinct functional groups, i.e., $-NO_2$, $-NH_2$, $-CH_3$, $-SO_2Cl$ and $-OH$, in groups of two and three into individual COPs. Notably, functionalizing COPs with multiple groups in one phase can lead to improved properties that are not simply linear combinations of those of the pure components. When two and three distinct functional groups are incorporated, i.e., $-NH_2$, $-SO_2Cl$ and $-OH$, into one phase, the multi-functionalized COP-21 and COP-22 exhibit an enhanced selectivity, roughly twice as large as that of any of the singly functionalized COPs. Therefore, incorporating multiple functional groups within a single COP may very well be useful for improving the carbon capture properties of a given material. Furthermore, at typical flue gas conditions both of these materials performed the best and displayed the lowest parasitic energies (1608 and 1632 kJ/kg) among all the frameworks studied, and of the singly functionalized frameworks, the amine functionalized COP-17 performed best. In a similar PPN study, it was observed that functionalizing the frameworks with longer amine chains improved their carbon capture performance. For these reasons, we anticipate that functionalizing the polymers presented here with longer amine chains that extend into the pore space will lead to further reduction in the parasitic energies of these frameworks. In summary, the controlled synthesis approach presented in this work opens up new possibilities for tuning the porous properties of porous organic polymers for a variety of applications, including the design of catalysts and functional sensors.

METHODS

Synthesis of Multifunctional COPs. **COP-21**: 1,5-Cyclooctadiene (cod, 0.50 mL, 3.96 mmol) was added to a solution of bis(1,5-cyclooctadiene)nickel(0) ([Ni(cod)2], 1.125 g, 4.09 mmol) and 2,2′-bipyridyl (0.640 g, 4.09 mmol) in dry DMF (65 mL), and the mixture was stirred until all solids completely dissolved. TBM (0.165 g, 0.262 mmol), DB-NH_2 (0.066 g, 0.262 mmol) and DB−OH (0.070 g, 0.262 mmol) were the comonomers, heated the reaction vessel at 85 °C to produce COP-21 powder (65 mg, 51% yield). Supercritical CO_2 drying process was used for activation. Elemental analysis calculated (%) for $C_{27}H_{25}ON$: C 85.44, H 6.64, N 3.69. Found (%): C 78.84, H 5.08, N 2.83. **COP-22**: All the experimental procedures are similar to those of the above COP-21 except for the comonomers (TBM (0.167 g, 0.262 mmol), DB-NH_2 (0.044 g, 0.174 mmol), DB−OH (0.047 g, 0.174 mmol) and DB-SO_2Cl (0.058 g, 0.174 mmol)). Heated the reaction vessel at 85 °C and activated with supercritical CO_2 to produce COP-22 powder (83 mg, 56% yield). Elemental analysis calculated (%) for $C_{111}H_{72}O_6N_2S_2Cl_2$: C 80.12, H 4.36, N 1.68, S 3.85. Found (%): C 78.52, H 5.357, N 1.923, S 3.745.

Prediction of Adsorption Selectivities of Binary Mixture by IAST. The single- and dual-site Langmuir adsorption model-based IAST has been applied to explore the adsorption selectivity of porous materials according to our previous method.[2b] The detailed information can be found in the Supporting Information. The selectivity for component x over component y can be evaluated from the predicted adsorption amount of each component of the mixture by the IAST theory using the following equation,

$$S_{i/j} = \frac{x_i/x_j}{y_i/y_j}$$

where x_i, x_j and y_i, y_j denote the molar fractions of species i and j in the adsorbed and bulk phases, respectively.

Parasitic Energy Calculations of a Binary Coal Flue Gas Mixture. The energy penalties have been estimated using the approach discussed by Huck et al.[2b] Parasitic energy is defined as

$$E_{\text{parasitic}} = 0.75\eta_{\text{carnot}}Q + W_{\text{comp}}$$

where Q and W_{comp} represent the heating and compression energy requirements, 0.75 corresponds to the typical turbine efficiency, and η_{carnot} is the Carnot efficiency for transforming heat into electrical energy. Further details on the energy estimation can be found in the Supporting Information and literature.[2b]

ASSOCIATED CONTENT

Supporting Information

The Supporting Information is available free of charge on the ACS Publications website at DOI: 10.1021/jacs.5b06266.

Generation of hypothetical COP-5 database structures. Experimental synthesis and characterization. Further details on the parasitic energy calculations. Prediction of adsorption of binary mixtures by IAST. Details on the application of the single- and dual-site Langmuir adsorption models by IAST to explore the adsorption selectivities of porous materials (PDF)

AUTHOR INFORMATION

Corresponding Authors

*caodp@mail.buct.edu.cn

*berend-smit@berkeley.edu

Notes

The authors declare no competing financial interest.

ACKNOWLEDGMENTS

This work is supported by National 863 Programs (2013AA031901, 2012AA101809), NSF of China (91334203, 21274011, 51502012) Scientific Research Funding (ZZ1304), Talent Funding (buctrc201420) from BUCT, Outstanding Talent Funding (RC1301) from BUCT, Talent cultivation of OIC (Nos. OIC201403003; OIC201503002), and the Fundamental Research Funds for the Central Universities (ZY1508). This research was also supported through the Center for Gas Separations Relevant to Clean Energy Technologies, an Energy Frontier Research Center funded by the U.S. Department of Energy, Office of Science, Office of Basic Energy Sciences under Award DE-SC0001015. This research used resources of the National Energy Research Scientific Computing Center, a DOE Office of Science User Facility supported by the Office of Science of the U.S. Department of Energy under Contract No. DE-AC02-05CH11231. Z.X. is thankful to Prof. J.F. Chen from IOC and Prof. L. M. Dai from Case Western Reserve University for helpful discussions.

REFERENCES

(1) Smit, B.; Reimer, J. R.; Oldenburg, C. M.; Bourg, I. C. *Introduction to Carbon Capture and Sequestration*; Imperial College Press: London, 2014.

(2) (a) Figueroa, J. D.; Fout, T.; Plasynski, S.; McIlvried, H.; Srivastava, R. D. *Int. J. Greenhouse Gas Control* **2008**, *2* (1), 9−20. (b) Huck, J. M.; Lin, L.-C.; Berger, A. H.; Shahrak, M. N.; Martin, R. L.; Bhown, A. S.; Haranczyk, M.; Reuter, K.; Smit, B. *Energy Environ. Sci.* **2014**, *7* (12), 4132−4146. (c) D'Alessandro, D. M.; Smit, B.; Long, J. R. *Angew. Chem., Int. Ed.* **2010**, *49* (35), 6058−6082.

(3) (a) Xiang, Z. H.; Cao, D. P. *J. Mater. Chem. A* **2013**, *1* (8), 2691−2718. (b) Xu, Y. H.; Jin, S. B.; Xu, H.; Nagai, A.; Jiang, D. L. *Chem. Soc. Rev.* **2013**, *42* (20), 8012−8031. (c) Dawson, R.; Cooper, A. I.; Adams,

DOI: 10.1021/jacs.5b06266
J. Am. Chem. Soc. 2015, 137, 13301−13307

D. J. *Prog. Polym. Sci.* **2012**, *37* (4), 530−563. (d) Patel, H. A.; Je, S. H.; Park, J.; Chen, D. P.; Jung, Y.; Yavuz, C. T.; Coskun, A. *Nat. Commun.* **2013**, *4*, 1357. (e) Ben, T.; Ren, H.; Ma, S.; Cao, D.; Lan, J.; Jing, X.; Wang, W.; Xu, J.; Deng, F.; Simmons, J. M.; Qiu, S.; Zhu, G. *Angew. Chem., Int. Ed.* **2009**, *48* (50), 9457−9460. (f) Yuan, D.; Lu, W.; Zhao, D.; Zhou, H.-C. *Adv. Mater.* **2011**, *23* (32), 3723−3725. (g) Xiang, Z. H.; Xue, Y. H.; Cao, D. P.; Huang, L.; Chen, J. F.; Dai, L. M. *Angew. Chem., Int. Ed.* **2014**, *53*, 2433−2437. (h) Xiang, Z. H.; Cao, D. P.; Huang, L.; Shui, J. L.; Wang, M.; Dai, L. M. *Adv. Mater.* **2014**, *26*, 3315−3320. (i) Pei, C.; Ben, T.; Li, Y.; Qiu, S. *Chem. Commun.* **2014**, *50* (46), 6134−6136.

(4) (a) Badi, N.; Lutz, J. F. *Chem. Soc. Rev.* **2009**, *38* (12), 3383−3390. (b) Gody, G.; Maschmeyer, T.; Zetterlund, P. B.; Perrier, S. *Nat. Commun.* **2013**, *4*, 2505. (c) Lutz, J. F.; Ouchi, M.; Liu, D. R.; Sawamoto, M. *Science* **2013**, *341* (6146), 628. (d) Bates, F. S.; Hillmyer, M. A.; Lodge, T. P.; Bates, C. M.; Delaney, K. T.; Fredrickson, G. H. *Science* **2012**, *336* (6080), 434−440.

(5) (a) Furukawa, H.; Cordova, K. E.; O'Keeffe, M.; Yaghi, O. M. *Science* **2013**, *341* (6149), 974. (b) Farha, O. K.; Eryazici, I.; Jeong, N. C.; Hauser, B. G.; Wilmer, C. E.; Sarjeant, A. A.; Snurr, R. Q.; Nguyen, S. T.; Yazaydın, A. Ö.; Hupp, J. T. *J. Am. Chem. Soc.* **2012**, *134* (36), 15016−15021.

(6) Feng, X.; Ding, X.; Jiang, D. *Chem. Soc. Rev.* **2012**, *41* (18), 6010−6022.

(7) Jiang, J.-X.; Su, F.; Trewin, A.; Wood, C. D.; Niu, H.; Jones, J. T. A.; Khimyak, Y. Z.; Cooper, A. I. *J. Am. Chem. Soc.* **2008**, *130* (24), 7710−7720.

(8) (a) Xiang, Z. H.; Cao, D. P.; Wang, W. C.; Yang, W. T.; Han, B. Y.; Lu, J. M. *J. Phys. Chem. C* **2012**, *116* (9), 5974−5980. (b) Lu, W. G.; Yuan, D. Q.; Zhao, D.; Schilling, C. I.; Plietzsch, O.; Muller, T.; Brase, S.; Guenther, J.; Blumel, J.; Krishna, R.; Li, Z.; Zhou, H. C. *Chem. Mater.* **2010**, *22* (21), 5964−5972. (c) Stöckel, E.; Wu, X.; Trewin, A.; Wood, C. D.; Clowes, R.; Campbell, N. L.; Jones, J. T. A.; Khimyak, Y. Z.; Adams, D. J.; Cooper, A. I. *Chem. Commun.* **2009**, 212−214.

(9) Holdren, J. P. *Materials Genome Initiative for Global Competitiveness*; National Science and Technology Council: Washington, DC, 2011.

(10) (a) Trewin, A.; Cooper, A. I. *Angew. Chem., Int. Ed.* **2010**, *49* (9), 1533−1535. (b) Thomas, J. M. H.; Trewin, A. *J. Phys. Chem. C* **2014**, *118* (34), 19712−19722. (c) Dawson, R.; Cooper, A. I.; Adams, D. J. *Polym. Int.* **2013**, *62* (3), 345−352.

(11) Pei, C.; Ben, T.; Qiu, S. *Mater. Horiz.* **2015**, *2* (1), 11−21.

(12) (a) Martin, R. L.; Shahrak, M. N.; Swisher, J. A.; Simon, C. M.; Sculley, J. P.; Zhou, H.-C.; Smit, B.; Haranczyk, M. *J. Phys. Chem. C* **2013**, *117* (39), 20037−20042. (b) Martin, R. L.; Simon, C. M.; Smit, B.; Haranczyk, M. *J. Am. Chem. Soc.* **2014**, *136* (13), 5006−5022.

(13) O'Keeffe, M.; Peskov, M. A.; Ramsden, S. J.; Yaghi, O. M. *Acc. Chem. Res.* **2008**, *41* (12), 1782−1789.

(14) (a) Liu, L. J.; Konstas, K.; Hill, M. R.; Telfer, S. G. *J. Am. Chem. Soc.* **2013**, *135* (47), 17731−17734. (b) Deng, H. X.; Grunder, S.; Cordova, K. E.; Valente, C.; Furukawa, H.; Hmadeh, M.; Gandara, F.; Whalley, A. C.; Liu, Z.; Asahina, S.; Kazumori, H.; O'Keeffe, M.; Terasaki, O.; Stoddart, J. F.; Yaghi, O. M. *Science* **2012**, *336* (6084), 1018−1023. (c) Eddaoudi, M.; Kim, J.; Rosi, N.; Vodak, D.; Wachter, J.; O'Keeffe, M.; Yaghi, O. M. *Science* **2002**, *295* (5554), 469−472.

(15) McKeown, N. B.; Budd, P. M.; Book, D. *Macromol. Rapid Commun.* **2007**, *28* (9), 995−1002.

(16) Jiang, J. X.; Su, F.; Trewin, A.; Wood, C. D.; Niu, H.; Jones, J. T. A.; Khimyak, Y. Z.; Cooper, A. I. *J. Am. Chem. Soc.* **2008**, *130* (24), 7710−7720.

(17) Deng, H. X.; Doonan, C. J.; Furukawa, H.; Ferreira, R. B.; Towne, J.; Knobler, C. B.; Wang, B.; Yaghi, O. M. *Science* **2010**, *327* (5967), 846−850.

(18) Han, S. S.; Goddard, W. A. *J. Phys. Chem. C* **2008**, *112* (35), 13431−13436.

(19) (a) Xiang, Z. H.; Leng, S. H.; Cao, D. P. *J. Phys. Chem. C* **2012**, *116* (19), 10573−10579. (b) Sumida, K.; Rogow, D. L.; Mason, J. A.; McDonald, T. M.; Bloch, E. D.; Herm, Z. R.; Bae, T.-H.; Long, J. R. *Chem. Rev.* **2012**, *112* (2), 724−781.

(20) Furukawa, H.; Yaghi, O. M. *J. Am. Chem. Soc.* **2009**, *131* (25), 8875−8883.

(21) Dawson, R.; Stockel, E.; Holst, J. R.; Adams, D. J.; Cooper, A. I. *Energy Environ. Sci.* **2011**, *4* (10), 4239−4245.

(22) Myers, A. L.; Prausnitz, J. M. *AIChE J.* **1965**, *11* (1), 121−127.

(23) Bae, Y.-S.; Snurr, R. Q. *Angew. Chem., Int. Ed.* **2011**, *50* (49), 11586−11596.

(24) Ziaii, S.; Rochelle, G. T.; Edgar, T. F. *Ind. Eng. Chem. Res.* **2009**, *48* (13), 6105−6111.

(25) Lin, L.-C.; Berger, A. H.; Martin, R. L.; Kim, J.; Swisher, J. A.; Jariwala, K.; Rycroft, C. H.; Bhown, A. S.; Deem, M. W.; Haranczyk, M.; Smit, B. *Nat. Mater.* **2012**, *11* (7), 633−641.

DOI: 10.1021/jacs.5b06266
J. Am. Chem. Soc. 2015, 137, 13301−13307